ACS APPLIED NANO MATERIALS

www.acsanm.org Article

Natural Wax-Stabilized Perovskite Nanocrystals as Pen-on-Paper Inks and Doughs

Sema Karabel Ocal, N. Burak Kiremitler, Ahmet Faruk Yazici, Nusret Celik, Evren Mutlugun,* and M. Serdar Onses*

Cite This: *ACS Appl. Nano Mater.* 2022, 5, 6201−6212 Read Online

ACCESS | Metrics & More | Article Recommendations | Supporting Information

ABSTRACT: Perovskite nanocrystals (PNCs) are emerging luminescent materials for a wide range of technological applications. The broad adaptation of PNCs will be greatly improved by addressing their intrinsically low stability and developing processes for their assembly into 2D and 3D structures using facile approaches. Inspired by the mechanism of natural protection of leaves, this paper proposes natural carnauba wax (CW) as an encapsulation material for PNCs. The synthesis of PNCs is performed in the presence of CW, which is derived from the leaves of *Copernicia prunifera* palm. CW acts as a solvent and replaces the commonly used octadecene in the preparation of PNCs. The facile synthesis in CW results in PNCs with greatly improved thermal, water, and air stability. Furthermore, the thermal and mechanical properties make PNC-Wax a highly suitable solid ink for versatile processing of these materials into 2D and 3D architectures. PNC-Wax can be printed via a pen-on-paper approach by heating at modest temperatures. The rapid plasticization of PNC-Wax by mechanical agitation enables hand-shaping of the material in a manner similar to playdoughs, which would possibly enable the versatile use of this material for various applications.

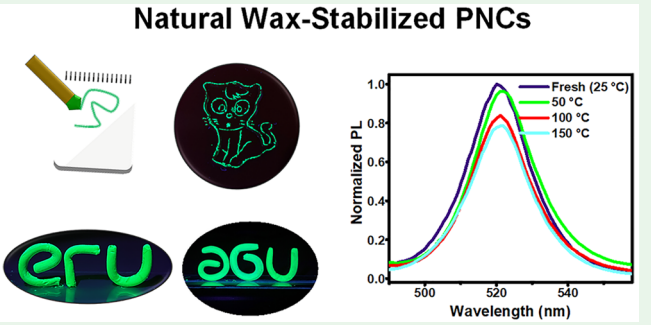

KEYWORDS: *perovskite nanocrystals, pen-on-paper, wax, photoluminescence, inks, doughs, encapsulation, stability*

INTRODUCTION

All-inorganic halide $CsPbX_3$ (X = Br, Cl, I, or mixed halide anions) perovskite nanocrystals (PNCs) have become attractive materials ever since a facile synthesis method was reported by Kovalenko and co-workers in 2015.[1] PNCs have exceptional properties, such as ultrahigh photoluminescence quantum yields (PLQYs, near-unity), a narrow emission full-width at half-maximum (FWHM; <20 nm), variable sizes and diverse shapes, cadmium-free, and a tunable peak emission wavelength throughout the entire visible spectrum.[1−6] As a result, PNCs have shown promising potential in various application fields including light-emitting diodes (LEDs),[7−9] lasers,[10,11] solar cells,[2,12−15] photodetectors,[16] optical communication,[17] backlit displays,[18] bioimaging,[19] photocatalysis,[20,21] and anticounterfeiting.[22−26]

Despite PNCs' outstanding properties, their applications are limited by the insufficient stability of these materials in various host media.[27] PNCs are vulnerable to environmental stress because of their inherently ionic nature, resulting in fast degradation under exposure to moisture, oxygen, light, heat, and polar solvents.[28,29] Therefore, achieving stable and high-quality PNCs in solution or in a polymeric form still remains a crucial challenge. So far, various strategies have been developed to improve the stability of PNCs. One of these strategies includes surface engineering for the passivation of PNCs with long-chained, branched, sterically hindered, cross-linked, or zwitterionic ligands[23,30−34] and the modification of these ligands by selective etching[35] or X-ray lithography.[36] However, most widely used ligands, such as oleic acid and oleylamine, can easily dissociate from the surface of PNCs. Other ligands require complicated synthesis techniques and tedious chemical processes. Among various approaches, encapsulating PNCs with protective inorganic (SiO_2,[37] glass,[17] Al_2O_3,[38] TiO_2,[39] ZrO_2,[40] ZnO,[41] zeolite,[42] metal−organic frameworks,[32] and geopolymers[43]) and organic (polystyrene,[44] poly(vinylidene fluoride),[45] poly(methyl methacrylate),[46,47] and block copolymers[48]) materials is widely studied as a practical and efficient strategy. There are some limitations of this encapsulation strategy, depending on the characteristics of the protective material. Inorganic shells and host matrixes are not dense enough because of high porosity. Sintering at high temperatures is performed to reduce the porosity; however, it is difficult to eliminate the morphological pinholes. Thus, they

Received: January 14, 2022
Accepted: April 7, 2022
Published: April 19, 2022

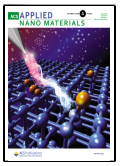

Downloaded via ABDULLAH GUL UNIV on February 28, 2023 at 07:49:36 (UTC).
See https://pubs.acs.org/sharingguidelines for options on how to legitimately share published articles.

© 2022 The Authors. Published by American Chemical Society

cannot completely protect PNCs from direct exposure to oxygen and moisture. Conversely, organic-based polymer matrixes offer fewer defect sites because they are more effective in the complete coverage of PNCs. A disadvantage of polymers is that they can easily degrade by thermal effects and display low stability under continuous light irradiation. The postsynthesis blending of PNCs with high-molecular-weight polymers requires long dissolution times, which inevitably result in the decomposition of PNCs due to prolonged oxygen or moisture exposure.[46] Apart from polymers, organic molecules based on fatty acid, such as stearic acid and paraffin, have also been used to enhance the stability of PNCs.[49,50] A common difficulty of the encapsulation strategy is the necessity for an additional postsynthesis step. The typical procedure involves the synthesis of PNCs followed by blending with a protective material through tedious centrifugation and washing processes to remove solvents such as octadecene (ODE) before blending. Thus, novel encapsulation strategies are required to overcome these challenges. An ideal encapsulation strategy should also enable the direct usage of materials as inks for versatile processing of PNCs into 2D and 3D architectures. This characteristic is particularly driven by the need for structured luminescent materials in practical applications. Security labels, for example, require the patterned deposition of luminescent materials.

In summary, the following characteristics are highly desirable for the effective encapsulation of PNCs. First, encapsulation should provide sufficient thermal, water, and air stability. Second, the encapsulation material should be readily available, low-cost, and nontoxic. In this regard, natural materials are of significant interest. Third, encapsulation should be directly achieved during the synthesis of PNCs without the need for an additional blending step. Fourth, the encapsulation material could serve multiple roles, minimizing the use of chemicals in the synthesis of PNCs. Finally, the resulting composites of PNCs should be readily processable as inks for the direct fabrication of 2D and 3D architectures.

Carnauba wax (CW) is a well-known low-cost, hydrophobic, and nontoxic natural material that demonstrates excellent physical and chemical stability, providing great protection against the degradation of drugs, bioactives, and foods. CW is found in the leaves of *Copernicia prunifera* palm. Such a wax coating encapsulates the leaves of the plant. This capability has inspired us to investigate the use of these materials in the encapsulation of PNCs. Herein, we propose a novel and facile strategy to synthesize highly stable and luminescent PNC-Wax by using CW not only as a protective matrix but also as a noncoordinating solvent that would serve as a medium that enables in situ nucleation and crystal growth during synthesis. Because of the protective nature of CW, fabricated PNC-Wax materials can be stored for months in solid or liquid form without a significant loss of their luminescence property, and they also present excellent water and thermal stability. We also demonstrated the direct usage of PNC-Wax inks as ready-to-use printable−writable solid inks for prospective applications such as pen-on-paper and anticounterfeiting. Moreover, PNC-Wax inks exhibit playdough-like properties, which allow one to use them as pliable free-standing 3D platforms. We envision that the stability performance and these interesting characteristics of PNC-Wax open exciting possibilities for future applications of PNCs.

EXPERIMENTAL SECTION

Materials. CW, cesium carbonate (Cs_2CO_3; 99%), lead bromide ($PbBr_2$; 99.9%), lead iodide (PbI_2; 99.9%), lead chloride ($PbCl_2$; 99.9%), 1-octadecene (ODE; 90%), oleic acid (OA; 90%), oleylamine (OAm; 80−90%), toluene (99.9%), *n*-hexane (95%), and acetone (95%) were purchased from Sigma-Aldrich. All reagents were used as received without further purification.

Preparation of Cesium Oleate (Cs-OA) Precursor. First, 3.9 g of Cs_2CO_3 was added with 48 mL of ODE and 12 mL of OA to a three-necked flask and vacuumed for 10 min. Then they were mixed followed by drying at 120 °C for 1 h. Once Cs-OA was obtained, it was cooled to room temperature and stored in a glovebox. All above reactions were carried out under an inert N_2 atmosphere. Because Cs-OA precipitates out of ODE at room temperature, it was preheated to 120 °C before injection.

Synthesis of PNCs in ODE. First, green PNCs ($CsPbBr_3$) were synthesized following the method developed by Kovalenko and co-workers[1] with some modifications. Briefly, 5 mL of ODE, 0.5 mL of OA, 0.5 mL of OAm, and 0.188 mmol of $PbBr_2$ were added to a 50 mL three-necked flask and dried under vacuum at 120 °C. After degassing, N_2 was used to fill the reaction flask and the temperature of the mixture was raised to 180 °C. After $PbBr_2$ dissolved completely, 0.4 mL of the Cs-OA solution (preheated to 120 °C) was swiftly injected into the reaction flask. A few seconds later, the flask was quickly cooled with an ice bath. All of the above reactions and processes were carried out under a N_2 atmosphere. The resultant solution was centrifuged at 5000 rpm and washed with *n*-hexane and acetone. The supernatant was discarded, and the precipitate was redispersed in toluene for further use. The blue- and red-emitting PNCs were synthesized by similar methods except that mixtures of $PbBr_2$−$PbCl_2$ (0.094 mmol of $PbBr_2$ + 0.094 mmol of $PbCl_2$) and $PbBr_2$−PbI_2 (0.075 mmol of $PbBr_2$ + 0.113 mmol of PbI_2) were used instead of $PbBr_2$ (0.188 mmol), respectively.

Synthesis of PNCs in CW (PNC-Wax). First, 3 g of CW was added to a 50 mL three-necked flask. The temperature was raised to 90 °C to melt CW. Then, 0.5 mL of OA, 0.5 mL of OAm, and 0.188 mmol of $PbBr_2$ were mixed with the CW melt under vacuum at 120 °C for 1 h to remove oxygen and moisture. After degassing, N_2 was used to fill the reaction flask and the temperature of the mixture was raised to 180 °C. A total of 0.4 mL of the Cs-OA solution preheated to 120 °C was swiftly injected into the reaction. A few seconds later, the flask was quickly cooled with an ice bath. The melting temperature of CW is 82 °C, and upon cooling to room temperature, PNC-Wax solidified. The resultant solid PNC-wax materials were taken out from flask and used directly in solid or colloidal form by dispersing it in toluene. Blue- and red-emitting PNC-Wax were also synthesized via the exact same synthesis steps, but instead of using $PbBr_2$, mixtures of $PbBr_2$−$PbCl_2$ (0.094 mmol of $PbBr_2$ + 0.094 mmol of $PbCl_2$) and $PbBr_2$−PbI_2 (0.075 mmol of $PbBr_2$ + 0.113 mmol of PbI_2) were used, respectively. Unless otherwise stated, green-emitting PNC-Wax was used throughout the paper.

Characterization. The morphology and particle size of PNC-Wax samples were observed by a FEI Tecnai G2 F20 S-TWIN high-resolution transmission electron microscope at 200 kV. The crystal structures were characterized by a Bruker AXS D8 X-ray diffractometer using copper radiation (λ = 1.5405 Å). Attenuated-total-reflection Fourier transform infrared (FTIR) spectra of the samples were obtained in the range of 400−4000 cm^{-1} using a spectrometer (PerkinElmer 400). Photoluminescence (PL) and absorbance spectra were measured using an Agilent-Cary Eclipse fluorescence spectrophotometer and a Thermo Genesys 10S spectrometer, respectively. Time-correlated single-photon-counting measurements were carried out using PicoQuant FluoTime 200 equipped with a 375 nm pulsed-laser diode. The wettability properties of PNC and PNC-Wax were evaluated by a Attension Theta Lite using static water contact-angle measurements. The hardness was measured by a Shore D hardness test. At least five measurements were made from different parts of the samples. To probe the mechanical properties, PNC-Wax was characterized by dynamic mechanical

https://doi.org/10.1021/acsanm.2c00224
ACS Appl. Nano Mater. 2022, 5, 6201−6212

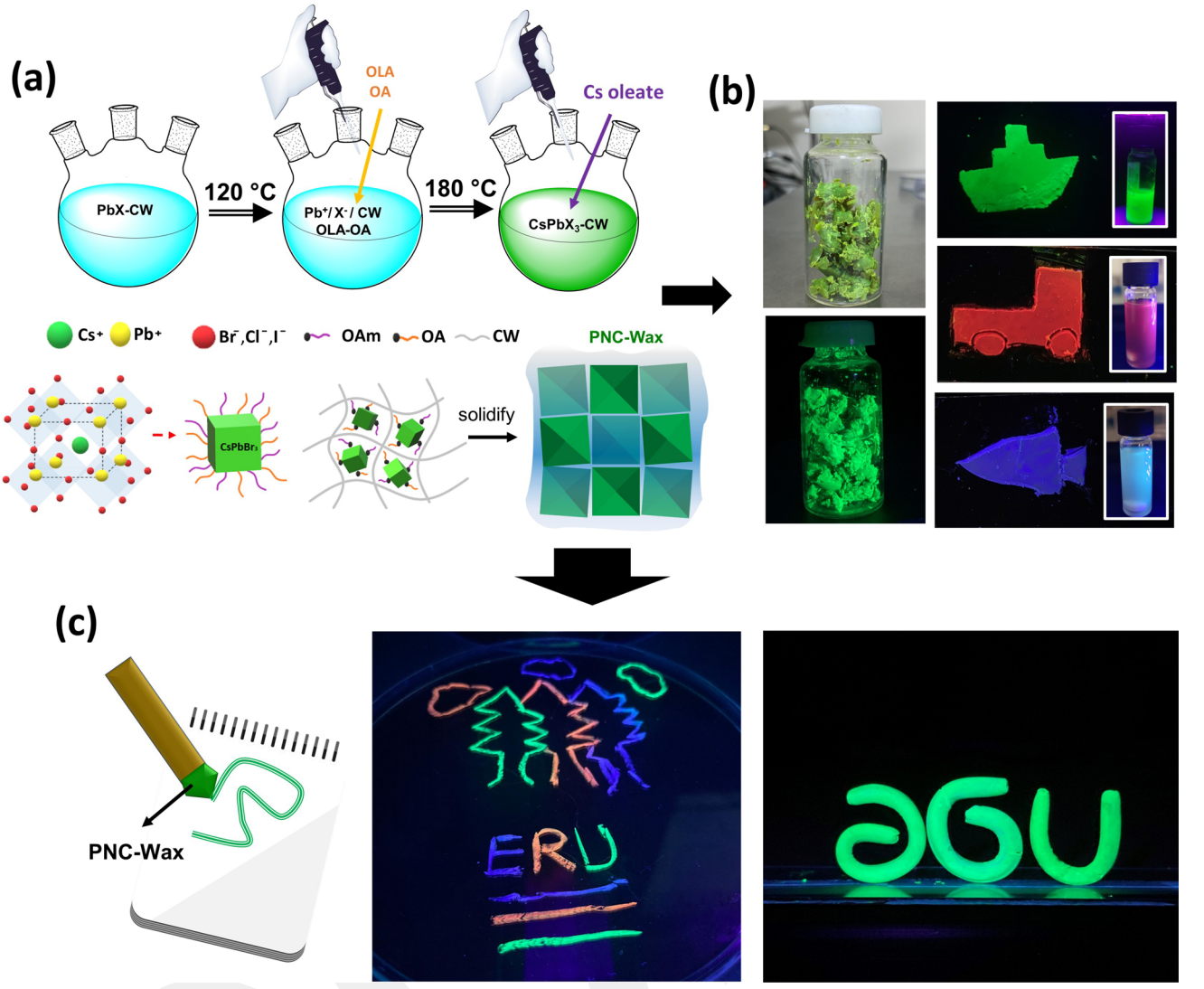

Figure 1. Synthesis and processing of PNC-Wax. (a) Schematic presentation of the synthesis steps and structure of PNC-Wax. (b) Photographs of the solid PNC-Wax materials obtained under UV and visible light and of the colloid form dispersed in toluene and the melt-cast film forms of green, red, and blue PNC-Wax. (c) Schematic illustration of pen-on-paper writing of PNC-Wax and drawings. On the right, 3D structures prepared by a playdough approach are presented.

analysis (DMA; PerkinElmer DMA 8000). For DMA, samples with a length of 20 mm and a diameter of 8.3 mm were prepared by hand kneading. The sample was tested by a single cantilever bending mode at a constant frequency of 1 Hz with a ramp rate of 2 °C min^{-1}. Thermogravimetric analysis (TGA) was performed by a thermal analyzer (PerkinElmer Pyris Diamond TGA/DTA). Measurements were carried out in an Ar atmosphere at a heating rate of 15 °C min^{-1} from room temperature to 550 °C.

Measurement of the Quantum Yield. The PLQY of PNC-Wax dispersed in toluene was measured by comparing it with an organic dye using the methodology reported in the literature.[51] Measurements on the solid films were performed by using a commercially available blue LED as the excitation source and a Hamamatsu C9920-12 EQE measurement system equipped with an integrating sphere. After collection of the blue LED spectrum inside the integrating sphere, the glass slide with a PNC film sample was placed on top of the LED. The next spectrum under the same experimental parameters was recorded. Comparing the corresponding portions of the integrals of both spectra gives the number of absorbed and emitted photons. The ratio of emitted-to-absorbed photon count yields the PLQY values of the PNC films.

Stability Tests. The stability of PNC-Wax in solid and colloidal forms was studied using different tests. Solid samples in thin films were prepared by melt-casting PNC-Wax onto a glass slide. Shaped films were obtained by hand carving around the film. To determine the long-term air stability, the PNC-Wax film formed on a glass slide was kept in room conditions for 3 months. To measure the water stability, the PNC-Wax films were immersed in water at room temperature and 60 °C for different times. The PNC-Wax films on glass slides were heated from 25 to 200 °C on a hot plate to determine their temperature stability. The stability of the PNC-Wax films was evaluated by monitoring the changes in the PL spectra of the films. To evaluate the ion migration/exchange stability, the PNC-Wax films were immersed in a KCl solution for durations of up to 120 h and changes in the resulting PL spectra were compared. The concentration of KCl was varied as 0.1, 1.0, and 2.0 M. To probe the photostability, the PNC-Wax film was exposed to a constant light flux with a peak wavelength of 397 nm by using a 3 mW UV flashlight driven by a power supply (Rigol DP712). The spectra were collected for 60 h at 6 h intervals.

PNC-Wax as Pen-on-Paper Inks and Playdoughs. PNC-Wax materials were processed into 2D and 3D architectures using pen-on-paper and playdough approaches. For the pen-on-paper approach, a small amount of PNC-Wax was melted onto a hot plate at 90 °C, and then the melt was plastered as a layer onto the tip of a pencil held on it. By subsequent rapid solidification of this layer, it was used as a pen-

https://doi.org/10.1021/acsanm.2c00224
ACS Appl. Nano Mater. 2022, 5, 6201−6212

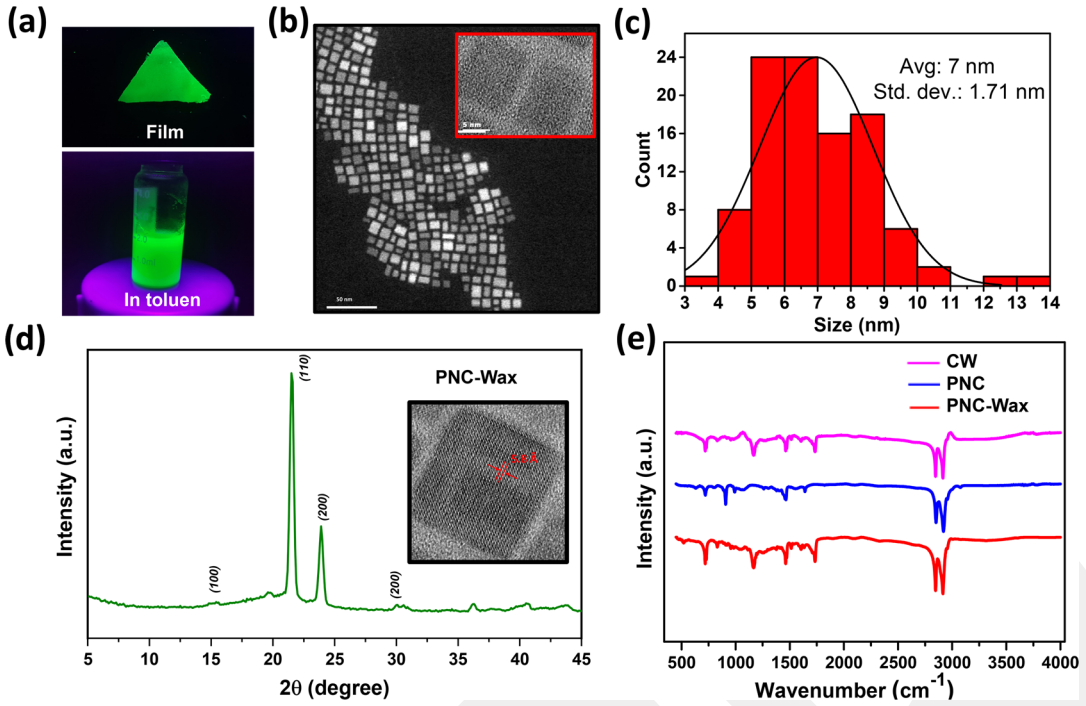

Figure 2. Characterization of the samples. (a) Photographs of green ($CsPbBr_3$) PNC-Wax samples in the colloid form dispersed in toluene and in a film formed by melt casting under UV exposure. (b) TEM and HRTEM (inset) images taken from the green PNC-Wax sample. (c) Size distribution histogram of the PNC-Wax nanocrystals. (d) XRD spectrum of the PNC-Wax film and HRTEM image of the PNC-Wax crystal (inset). (e) FTIR spectra of PNC, CW, and PNC-Wax.

on-paper solid ink similar to crayons by direct writing onto various surfaces such as plastics and banknotes. For a demonstration of the direct melt printing application, PNC-Wax solid cartridges were melt-printed onto surfaces using a glue pen (Bosch Gluey). The cartridges suitable for the glue pen (20 mm length and 7 mm radius) were prepared by hand kneading and shaping of PNC-Wax pigments. Direct melt writing was performed with PNC-Wax ink manually fed to the printing tip at an operation temperature of the device of 150 °C. For the fabrication and demonstration of playdough-like-shapeable, 3D free-standing objects, PNC-Wax materials were kneaded by hand and shaped in the form of letters.

RESULTS AND DISCUSSION

Figure 1 presents a schematic illustration of the synthesis and potential applications of PNC-Wax. PNCs were encapsulated in CW during the synthesis. The choice of CW stems from several reasons: (i) Solid CW is a nontoxic, low-cost, and a natural material. Unlike other waxes such as paraffin and beeswax, its higher melting point of 80−85 °C offers a suitable operating temperature for applications. (ii) Solid CW exhibits hydrophobic and antioxidant properties, providing effective protection of PNCs against water and oxygen. (iii) It can act as an appropriate solvent and medium to dissolve lead sources and colloidally disperse PNCs. The synthesis is schematically depicted in Figure 1a. First, appropriate amounts of PbX_2, OAm, and OA were dissolved in a certain amount of molten CW. PNCs of $CsPbX_3$ were subsequently in situ synthesized after hot injection of the Cs-OA precursor into the mixture. It should be noted that no solvent other than melt CW was used in this process; i.e., CW was used not only as an encapsulation agent but also as a solvent. Unlike the usual encapsulation strategies that are generally applied after postsynthesis, the direct in situ use of CW is one of the peculiarities of our study and allows the use of a minimum amount of solvent. PNC-Wax materials can solidify quickly after synthesis, enabling their direct usage without the need for tedious centrifugation and washing procedures. Besides the simplicity, the preparation of materials without additional purification steps further contributes to the sustainability of the process. We have shown the use of the green, red, and blue PNC-Wax materials in colloidal form by dispersing them directly into suitable solvents. Alternatively, they can be processed into a film by melting and then coating them onto the surfaces. PNCs are homogeneously dispersed inside wax without any visible agglomeration. Correspondingly, PL measurements performed from different positions of a PNC-Wax film, as given in Figure S1, showed that there is only a 3% difference between the minimum and maximum values for the integrated spectra. An inherent advantage of the proposed approach is the ability to process these materials into 2D and 3D structures using facile pen-on-paper and playdough methods (Figure 1c).

Figure 2 presents the key structural and chemical properties of green-emitting PNC-Wax materials. Visually, PNC-Wax exhibits strong PL (Figure 2a) in the colloidal and film forms under the excitation of 365 nm light. The size and morphology of the as-prepared green PNC-Wax materials were investigated through transmission electron microscopy (TEM). As shown in Figure 2b,c, cubic-shaped PNCs, with an average size of 7 ± 1.71 nm, were obtained. The interplanar spacing of 5.8 Å measured from the high-resolution TEM (HRTEM) images (inset of Figure 2d) fits the (100) crystal plane of the orthorhombic PNC-Wax.[1] The crystal structures of PNC and PNC-Wax thin films were confirmed by the X-ray diffraction (XRD) patterns shown in Figure 2d. The XRD analysis results of PNC, CW, and PNC-Wax are provided in Figure S2. The orthorhombic crystals of CW manifested themselves as two strong diffraction peaks at 2θ = 21.5° and 23.9°, which were assigned to the (110) and (200) planes, respectively.[52,53] The characteristic peaks at 2θ = 14.7°, 21.5°, and 30.1° refer to the

https://doi.org/10.1021/acsanm.2c00224
ACS Appl. Nano Mater. 2022, 5, 6201−6212

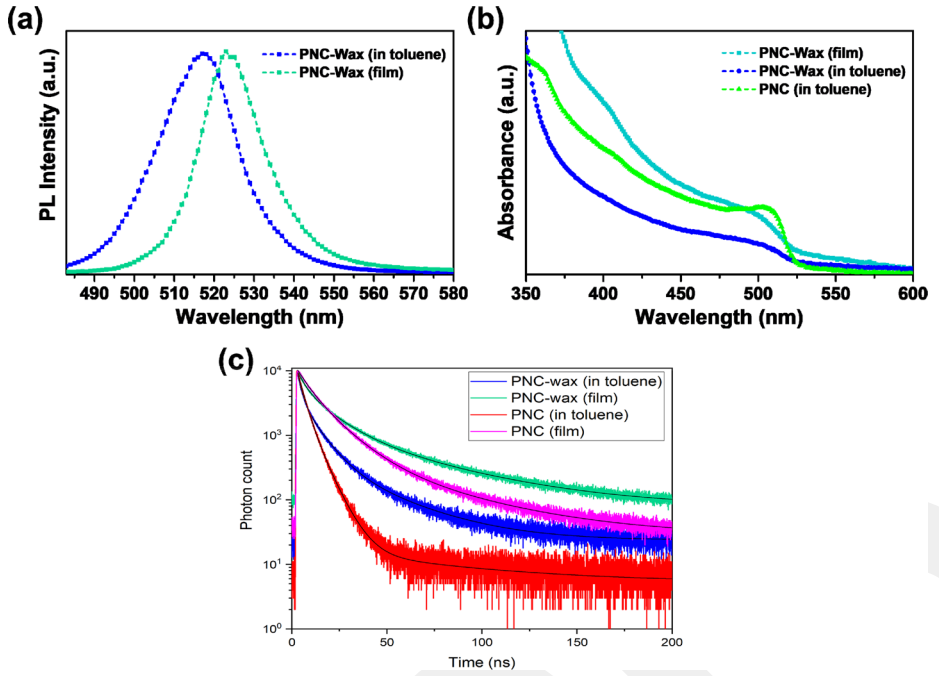

Figure 3. Optical properties of PNC and PNC-Wax. Comparison of the (a) steady-state PL spectra of PNC-Wax in the film and colloidal dispersion forms, (b) absorption spectra, and (c) TRPL spectra of PNC and PNC-Wax in the film and colloidal dispersion forms.

Table 1. Lifetime Components of PNC and PNC-Wax

	PNC		PNC-Wax	
	in toluene	film	in toluene	film
A_1	14.4 ± 2.3	580.6 ± 13.7	466.6 ± 14.1	1266.0 ± 16.3
τ_1 (ns)	67.2 ± 8.6	46.2 ± 0.7	30.7 ± 0.6	49.1 ± 0.5
A_2	3100.6 ± 63.2	5594.1 ± 56.8	3524.3 ± 59.6	4508.0 ± 55.6
τ_2 (ns)	6.9 ± 0.1	13.8 ± 0.1	8.6 ± 0.1	14.0 ± 0.2
A_3	7009.0 ± 134.0	4086.0 ± 113.0	6023.0 ± 190.0	4222.0 ± 142.0
τ_3 (ns)	3.2 ± 0.1	5.8 ± 0.2	2.0 ± 0.1	3.8 ± 0.1
$\tau_{average}$ (ns) (amplitude-weighted)	4.5	12.5	5.7	14.1

(100), (110), and (200) planes of orthorhombic $CsPbBr_3$ crystals. These peaks are in good agreement with PNCs synthesized by the typical hot-injection method.[1] Because of the compatibility of the orthorhombic crystal structures of both PNC and solid wax, it can be deduced that these materials form a homogeneous and therefore stable mixture that is synergistically compatible.

In the FTIR analysis given in Figure 2e, distinct vibration bands related to polar functionalities such as carbonyls and unsaturated ester groups can be observed for the samples that contain CW. These bands located at 1730−1750 and 1160−1175 cm^{-1} for the CW and PNC-Wax samples are in good agreement with the literature;[54,55] meanwhile, they are not found in the spectrum of PNC, which is synthesized by the typical hot injection. On the other hand, the characteristic bands of ODE used in the synthesis of PNC at 800−1000 and 3000−3100 cm^{-1}, indicating out-of-plane character of the vinyl group of C−H and C−H stretching, respectively,[56] can be clearly detected in the PNC sample; however, these bands are not visible for the PNC-Wax sample because only a very low amount of ODE is used during the addition of the Cs-OA precursor.

Figure 3 presents the optical properties of PNC-Wax measured by using steady-state PL and time-resolved photoluminescence (TRPL) spectroscopy. PL spectra of green PNC-Wax in the film and colloidal forms exhibit quite narrow (FWHM of around 21 nm) emission peaks centered at 517 and 523 nm, respectively. Energy transfer among the PNCs is more likely to occur in the film form because of the close-packed structure. This phenomenon is reflected in the PL spectrum as a ∼6 nm red shift in the PNC-Wax film. The PLQY of the obtained green PNC-Wax film was calculated as ∼70%. As seen from the absorption spectra taken from colloidal PNC and PNC-Wax in the colloidal dispersion and film forms (Figure 3b), the absorbance values of the samples are consistent with each other. The TRPL measurement results, as given in Figure 3c and Table 1, reveal that, because the samples were prepared in a film form, elongated lifetimes were observed, which indicates suppression of the fast decay components, i.e., the nonradiative-transfer channels.

It is widely predictable that PNCs are susceptible to severe oxidation in an ambient environment and are highly degraded by elevated temperatures and light exposure. We put forth that an encapsulation and in situ crystallization strategy of PNCs via CW offers great advantages to these stability issues. PNC-Wax exhibits satisfactory ambient air stability. For the long-term air stability test, the PL intensity was first measured immediately after the synthesis and the PLQY was calculated.

https://doi.org/10.1021/acsanm.2c00224
ACS Appl. Nano Mater. 2022, 5, 6201−6212

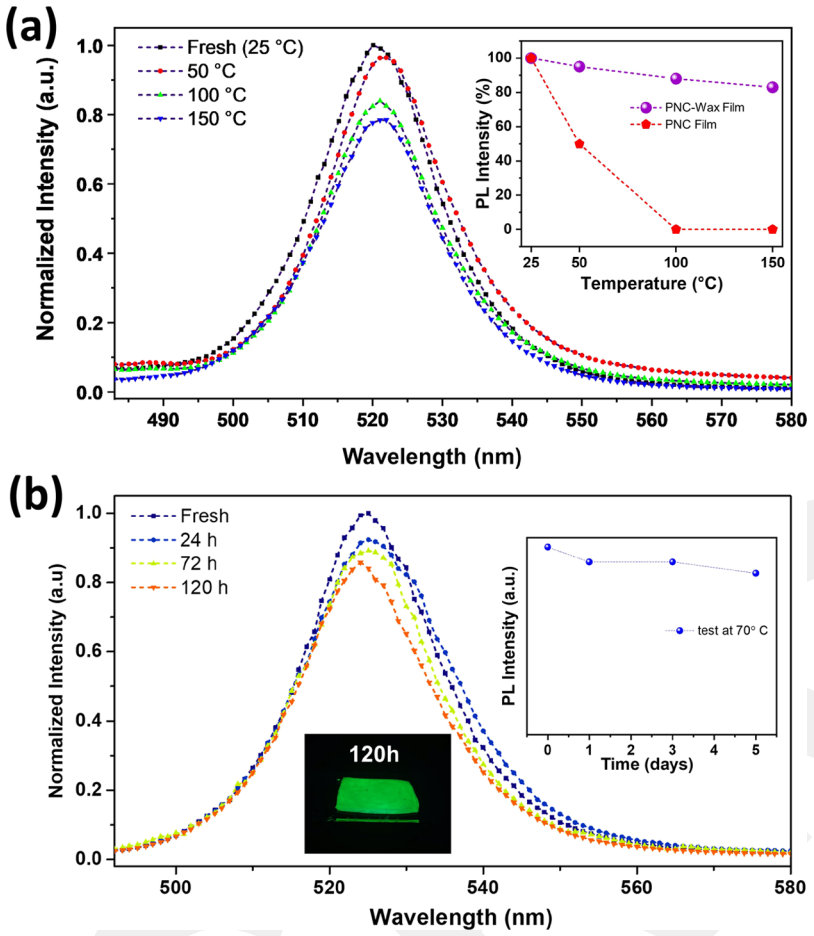

Figure 4. Thermal stability of the PNC-Wax films. (a) Comparison of the PL spectra after treatment of the PNC-Wax film exposed to different temperatures for 5 min. Inset: Comparison of the relative PL intensities of the PNC and PNC-Wax films under the same conditions. (b) Comparison of the PL spectra and relative PL intensity (inset) taken after long-term treatment of the PNC-Wax film at a constant temperature of 70 °C for 1−5 days. Inset: Photograph of the PNC-Wax film under UV irradiation after heat treatment for 5 days.

The measurement was repeated 3 months after storage in ambient air. The results (Figure S3) showed that PNC-Wax retained 83% of the initial PL intensity and PLQY exhibited a partial decrease to 51%. To further probe the photostability, the PNC-Wax film was tested under constant exposure to UV flux. According to the real-time PL measurements (Figure S4), steady-state decays in the emission intensity ratio were determined as approximately 9%, 17%, 27%, and 39% for samples exposed to UV light for 12, 24, 36, and 60 h, respectively.

Another important consideration for PNCs is the thermal stability. To probe the thermal stability, the PL intensities of the films of PNC and PNC-Wax were measured upon treatment at different temperatures and durations. Figure 4a presents the PL spectra of the samples heated at temperatures of 50, 100, and 150 °C for 5 min. For the pristine PNC film, the PL significantly decreased upon thermal treatment even at a short time. At a treatment of 50 and 100 °C, the PL intensity reduced to 50% and 100% of the initial value, respectively. In strong contrast, the PNC-Wax film exhibited much higher thermal stability with only 3% decay in the PL intensity for thermal treatment at 50 °C for 5 min. The PL of PNC-Wax was greater than 80% of the initial value for thermal treatment at 100 and 150 °C. Note that these temperatures are higher than the melting temperature (82 °C) of CW and the PNC-Wax film exhibits a change in its shape upon treatment. The bright PL, together with the change in shape, can be clearly seen in photographs (Figure S5) taken under UV-light excitation. The thermal stability of PNC-Wax at the melt state facilitates facile processing of these photoluminescent materials as solid inks for pen-on-paper applications, as demonstrated in the following parts of this study. In addition to these tests, the PNC-Wax film was subjected to a cyclic heating−cooling test (Figure S6). PNC-Wax was heated to 200 °C for 10 min and then cooled to room temperature, and PL measurement was done. During heating, CW melted at temperatures higher than its melting temperature of 82 °C. The PNC-Wax film retained about 80% and 60% of its original PL intensity after 2 and 10 heating−cooling cycles, respectively. This characteristic is particularly advantageous for melt-printing applications.

For practical applications, the long-term stability of PNCs at modest temperatures is important. A photoluminescent material in a product, for example, can experience high temperature during transport over different regions of the world. Considering the typical daily temperatures and melting point of CW, we studied the long-term stability at a temperature of 70 °C. Figure 4b presents the PL spectra for PNC-Wax, which was heated at 70 °C for up to 5 days. At this temperature, the PNC-Wax film retained its integrity throughout the experiment. There was only limited (<20%) degradation in the PL behavior of PNC-Wax even after 5 days

https://doi.org/10.1021/acsanm.2c00224
ACS Appl. Nano Mater. 2022, 5, 6201−6212

Table 2. Comparison of Stability Characteristics of PNCs Reported in the Literature

sample	PLQY (%)	water stability (%; relative PL)	air stability (%; relative PL)	thermal stability (%; relative PL)
$CsPbBr_3$/PMMA (PBMA)[46]	54.6–62.2	~79–82 (1 day)	70, 78 (1 month)	~82.6 (1 day, in a N_2 atmosphere)
$CsPbBr_3$@PMMA/PEI[57]	~75	80 (40 days)	>95 (2 months)	70 (6 heating–cooling cycles at 25/120 °C)
$CsPbBr_3$@PS fibers[44]	48	70 (8 days)	NA	50 (80 °C, 120 min)
$MAPbBr_3$/PQDP[58]	59.4	>90 (100 days, 60% RH)	>90 (2 months, 16 W UV)	>60 (100 °C, 60 days)
P-g-PQDs[50] ($CsPbBr_3$@paraffin)	44.7	78 (20 days)	75 (20 days)	NA
$CsPbBr_3$PeQD/Ergo film[59]	38	91 (1 day)	81 (1 month)	NA
$CsPbBr_3$@SiO_2 matrix[60]	68	NA	94.3 (1 month)	72% (105 °C, 2 cycles)
PNC ($CsPbBr_3$)-Wax (this work)	68–70	91 (1 day) 70 (5 days, 25 and 60 °C) 50 (20 days, 60 °C)	83 (3 months)	>80 (5 days, 70 °C) 83–80 (100–150 °C) 80 (2 cycles), 60 (10 cycles) (200 °C)

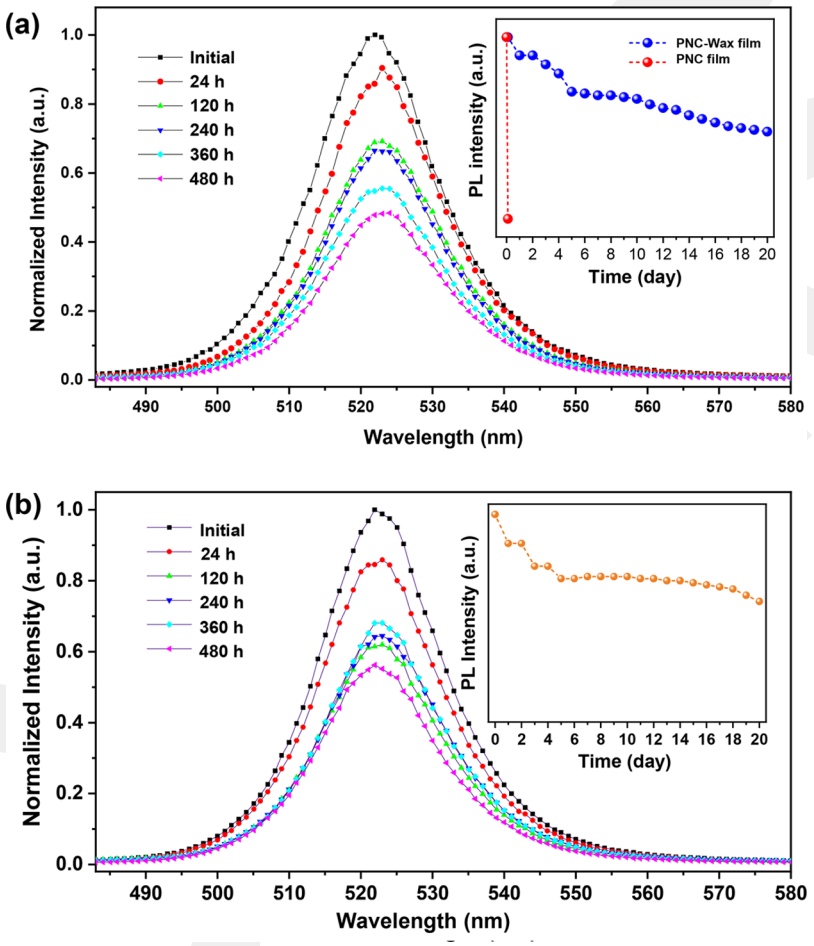

Figure 5. Water stability tests. (a) Comparison of the PL spectra after immersing the PNC-Wax film in water at room temperature for 1–20 days. Inset: Comparison of the relative PL intensities of the PNC and PNC-Wax films under the same conditions. (b) Comparison of the PL spectra and relative PL intensities (inset) taken after immersing the PNC-Wax film in water at a constant temperature of 60 °C for 1–20 days.

of exposure to 70 °C. The slight changes in the PL peak-emission wavelength and FWHM were due to modification of the initial conditions, i.e., built-up moisture, thermal stress, etc., giving rise to modified excitonic transitions at the film. The narrowing of the PL therefore can be attributed to partial passivation of the size- and/or stoichiometry-dependent emission among the PNC-Wax film in an uncontrolled manner. In summary, to the best of our knowledge, our strategy possesses one of highest thermal stabilities for PNC materials (Table 2). Another important point is that there is no significant shift in the wavelength of the maximum PL for all of the thermal stability experiments, although it should be noted that a negligible slight change in the PL peak emission was observed for the long-term test (Figure 4b).

In an effort to simulate the conditions that can be encountered in the applications, the water stability was studied. For this purpose, pristine PNC and PNC-Wax films were immersed in water at room temperature and 60 °C up to 20 days (Figure 5). For pristine PNC films, the PL completely disappeared after immersion in water for 2 h. In strong contrast, the PL of the PNC-Wax film was highly stable and decreased only 9% after immersion in water for 1 day. Even after 20 days, the PNC-Wax film still appeared to be strongly emissive without exhibiting a significant reduction in fluorescence (Figure 5a and inset). A similar water stability

https://doi.org/10.1021/acsanm.2c00224
ACS Appl. Nano Mater. 2022, 5, 6201–6212

performance was observed for the PNC-Wax film immersed in water at a temperature of 60 °C (Figure 5b). These results imply that PNC-Wax exhibits a high level of water stability. In addition to the water stability, it is known that PNCs are highly vulnerable to ion exchange when exposed to halogen ions. To determine the ion migration/exchange stability, PNC-Wax films were immersed in KCl solutions of varying concentration and time-dependent PL measurements were taken (Figure S7). The results showed that the film exposed to chlorine ions for 120 h was highly resistant to ion exchange. The maximum peak wavelength did not shift, and the PL decreased at a rate slightly higher than those tested in pure water.

The greatly improved stability of PNC-Wax stems from the intrinsic properties of CW and an in situ encapsulation approach. The poor stability of PNCs is attributed to their ionic nature, which results in ion migration and structural instability. The capping ligands (OA and OAm) used in the synthesis of PNCs tend to interact with the nanocrystal surface with their carboxylate and alkylammonium groups; the carboxylates bond with the surface lead atoms, while the alkyl groups interact with the surface bromide via hydrogen bonding [Br···N−H$^+$].[61] Polar solvents such as water degrade [Br···N−H$^+$] hydrogen bonding because it is weaker than metal−ligand interaction.[62] However, CW is a hydrophobic material[63] that contains a complex mixture mainly composed of aliphatic esters, diesters of 4-hydroxycinnamic acid, and esters of ω-hydroxycarboxylic acid. The CW molecules encapsulate the PNCs efficiently during synthesis. The crystal structure of the CW solidified after synthesis and that of the PNC match each other so that the PNCs are strongly caged, thus enabling great improvement in the stability. The excess ligands and byproducts can also contribute to the stability of PNC-Wax. Because of the hydrophobicity, CW possibly prevents moisture and oxygen penetration to the surfaces of the nanocrystals. As shown in Figure S8, while the pristine PNC film exhibited hydrophilic character with a water contact angle (CA) of 62°, the PNC-Wax film was highly hydrophobic with a contact angle of 112°. During synthesis, CW acts as a noncoordinating solvent, and the hydroxyl and carbon nucleophile groups may serve as protonation supplies for environmental oxygen and moisture, enabling protection from breakage of [Br···N−H$^+$] hydrogen bonding, and thus can strengthen the loosely bound ligands around the PNCs.[64] Overall, PNC-Wax exhibits outstanding stability against air, heat, and water moisture. In Table 2 some examples of the latest state-of-the-art strategies are compared with our study.

Apart from their high stability and ease of synthesis, PNC-Wax materials show great promise for pen-on-paper and dough applications. Benefiting from the thermal stability of PNC-Wax materials in the melt state, we first explored the use of PNC-Wax as a solid ink for the direct writing of luminescent patterns. Figure 6 presents a summary of these experiments. The PNC-Wax material was melted on a hot plate at 90 °C, and then the melt was plastered as a layer onto the tip of a pencil held on it. The rapid solidification of PNC-Wax allows for the direct application of PNC-Wax onto the surface of a material in the desired macroscopic pattern. The photoluminescent patterns of multiple colors can be written in a manner similar to crayons. The writing can be performed on different substrates such as plastics (Figure 6b and Supporting Video S1) and banknotes (Figure 6c). Such photoluminescent patterns can be used as security labels for encoding information. In this context, PNC-Wax can be easily produced,

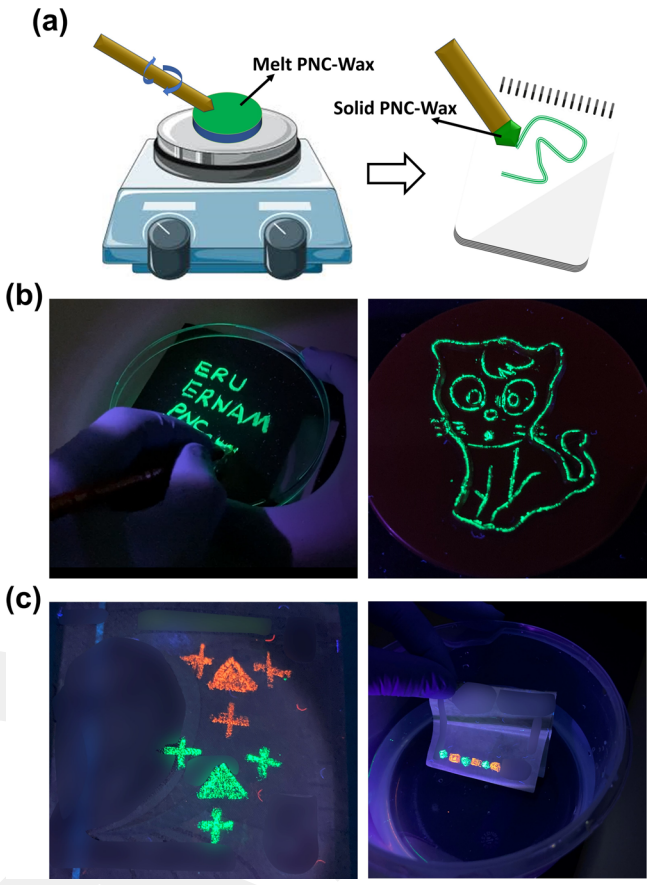

Figure 6. Pen-on-paper applications of PNC-Wax. (a) Schematic illustration of the process. Left: Melting and plastering PNC-Wax onto the tip of a pen. Right: Direct writing of PNC-Wax on surfaces by subsequent rapid solidification. (b) Photographs showing the direct printing of PNC-Wax inks in the form of letters and shapes on plastic substrates. The photograph was taken under UV excitation (see Supporting Video S1). (c) Photographs showing banknotes with various patterns of green- and orange-emitting PNC-Wax. The photograph on the right shows a banknote immersed in water (see Supporting Video S2).

have high stability in an external environment, be applied directly to various surfaces in an additive way, and have multicolored luminescence, which offers great potential in terms of being integrated into anticounterfeiting applications as security inks. As a demonstration of this potential, we drew freeform symbols on the banknote surface using green- and orange-emitting PNC-Wax solid inks. In Figure 6c and Supporting Video S2, it is also demonstrated that the labels drawn with PNC-Wax solid inks preserve their integrity and PL even after immersion in water.

To further demonstrate the practical utility of PNC-Wax inks, we explored direct writing using commercial glue pens. Waxes are widely used phase-change materials[65] that are solid at room temperature and can be melted into a reservoir, where it becomes liquid upon heating. This characteristic makes them suitable solid inks for pen-on-paper and drop-on-demand additive fabrication techniques such as wax printing, 3D printing, or electrohydrodynamic jet printing.[66,67] Figure 7 presents a schematic illustration and the key results on the use of PNC-Wax as inks in a commercial glue pen. Thanks to the ease of formability, cartridges consisting of solid PNC-Wax of a suitable size can be readily prepared and inserted into the glue

https://doi.org/10.1021/acsanm.2c00224
ACS Appl. Nano Mater. 2022, 5, 6201−6212

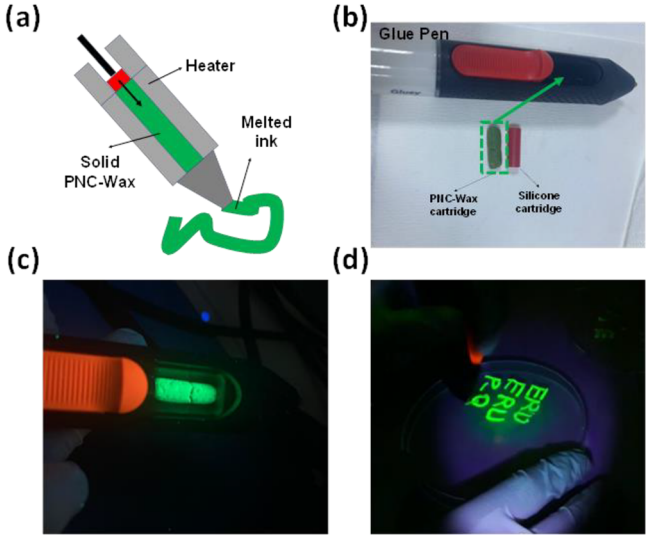

Figure 7. Direct melt printing of PNC-Wax solid inks. (a) Schematic illustration of the process using a glue pen. (b) Photograph showing the glue pen and solid form PNC-Wax cartridge used for direct melt writing. (c) Photograph of the glue pen with an inserted PNC-Wax cartridge under UV light. (d) Photograph taken during direct-melt-writing operation of PNC-Wax under UV light (also see Supporting Video S3).

pen reservoir. The thermal stability of PNC-Wax ensures retainment of the PL properties during printing at a constant operating temperature of 150 °C. The molten PNC-Wax ink immediately solidifies upon contact with the surface. The immediate solidification allows the writing of patterns without spreading (Figure 7a and Supporting Video S3). These demonstrations show great promise for further exploration of the direct writing of PNC-Wax materials using different printer systems.

As a final demonstration, we exploit the unique mechanical properties of the PNC-Wax materials for making photoluminescent macroscopic shapes. We found that the PNC-Wax material softens when subjected to mechanical deformation and can be easily formed into a free-standing 3D object. This behavior is similar that of playdoughs, which are cohesive and malleable materials that can be shaped by hand. Waxes, including CW, can undergo solid−solid phase transformation at temperatures below their melting temperature, and together with their high heat storage capacity and low thermal conductivity,[68,69] they can transform from a relatively rigid solid to a softer solid at increasing temperatures with a mechanical effect. Normally, bulk CW is more rigid and brittle than other waxes, so it is difficult to take shape even at softening conditions. On the other hand, OA and OAm, which are used as surfactants and stabilizers for the in situ synthesis, act as plasticizers at the same time, thereby increasing the softening and thus formability of PNC-Wax by mechanical and thermal effects. To further probe these effects, the average Shore D hardness values were found to be 49.5 ± 6.4 and 20.4 ± 3.5 for bulk CW and PNC-Wax, respectively. Besides that, as can be seen in the results of the TGA provided in Figure S9, the extra weight loss between 150 and 250 °C shown by PNC-Wax compared to pure CW likely relates to the presence of OA and OAm in the structure. As presented in Figure 8, we simply softened the as-synthesized PNC-Wax materials by hand kneading (Figure 8a,b) and then shaped them to 3D objects

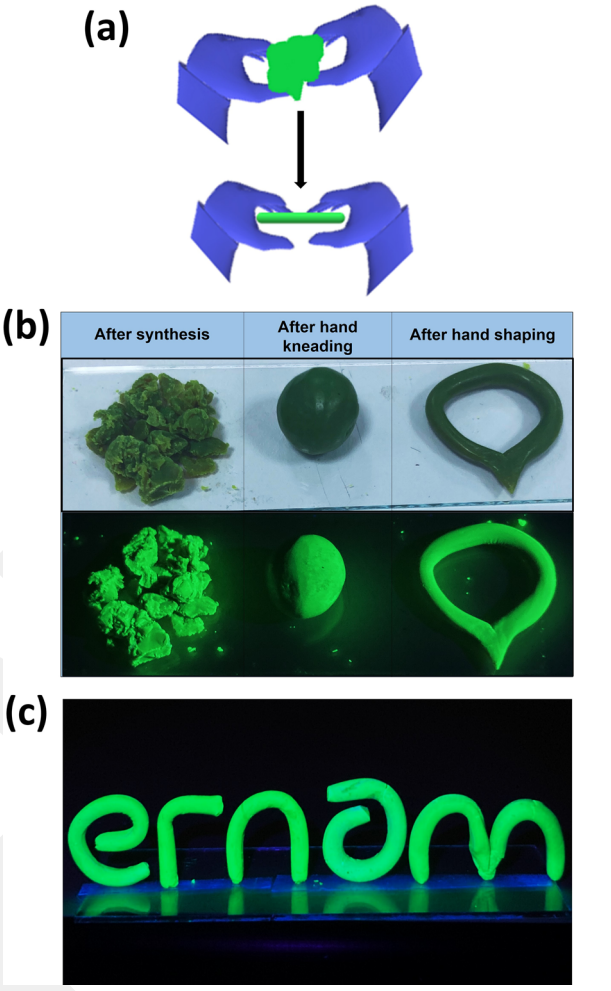

Figure 8. PNC-Wax doughs. (a) Representative figure showing the hand kneading of PNC-Wax materials. (b) Normal and UV-light photographs of PNC-Wax after synthesis, hand kneading, and hand shaping. (c) Photographs of macroscopic 3D structures.

(Figure 8c). As the kneading time is increased, the temperature measured from the surface of PNC-Wax can reach around 45 °C as result of the stored heat. Its poor thermal conductivity extends its ability to maintain heat, thus extending the formability period. Alternatively, kneading can be done on a hot plate at temperatures of 40−50 °C for a shorter softening time. To reveal the mechanical properties as a function of the temperature, PNC-Wax was characterized by DMA. According to the DMA shown in Figure S10, both the storage modulus (E') and loss modulus (E'') decrease with increasing temperature. The significant plasticity induced by softening was observed after around 65 °C, where the tan δ (E''/E') value increased with a steep slope, while the solid−liquid transition started around 78 °C, the temperature at which E' and E'' coincide. Apart from that, the slight bump observed at the tan δ value around 35−45 °C can be identified as the solid−solid transition region, which indicates the malleability of PNC-Wax doughs in this temperature range.

Obtained free-standing objects appear to be strongly photoluminescent and reusable. As a result, the obtained PNC-Wax materials can be directly shaped without the need for any additional processing. The ease of generating 3D objects should open up new opportunities for a wide range of applications.

https://doi.org/10.1021/acsanm.2c00224
ACS Appl. Nano Mater. 2022, 5, 6201−6212

CONCLUSIONS

In summary, this study reported the in situ encapsulation of PNCs with a natural wax material. The encapsulation is performed during the synthesis of PNCs using wax as a replacement for the ODE solvent. There are two key outcomes of the presented approach. First, the wax greatly improves the thermal and water stability of PNCs. Second, the resulting PNC-Wax material enables facile processing of photoluminescent materials into 2D and 3D macroscopic architectures. The modest melting temperature and stability enhancement of wax provide direct printing from melt. This capability is useful for generating photoluminescent patterns of PNCs using a pen-on-paper approach. The solid inks composed of PNC-Wax offer strong promise for use with other advanced forms of printing. The interesting mechanical properties of PNC-Wax provide high levels of malleability. As a result, PNC-Wax can behave like a dough and be formed into desired shapes by hand kneading, similar to playdoughs. This latter capability can be explored with other nanomaterials in future studies. PNC-Wax shows great potential in melt-printing applications to generate 2D and 3D architectures. The replacement of an organic solvent with a nontoxic natural material further contributes to the sustainability aspect of the process.

ASSOCIATED CONTENT

Supporting Information

The Supporting Information is available free of charge at https://pubs.acs.org/doi/10.1021/acsanm.2c00224.

Additional XRD data, photostability of the PNC-Wax film, additional photographs and PL spectra from thermal and ion-exchange stability tests of the PNC-Wax film, contact-angle measurements, and TGA and DMA results (PDF)

Video S1 of a direct printing demonstration of PNC-Wax inks on a plastic substrate (MP4)

Video S2 of a demonstration of underwater durability on a banknote with printed PNC-Wax inks (MP4)

Video S3 of a direct melt-printing demonstration of PNC-Wax inks on a plastic substrate (MP4)

AUTHOR INFORMATION

Corresponding Authors

M. Serdar Onses − *ERNAM—Nanotechnology Research and Application Center, Erciyes University, Kayseri 38039, Turkey; Department of Materials Science and Engineering, Erciyes University, Kayseri 38039, Turkey; UNAM—Institute of Materials Science and Nanotechnology, Bilkent University, Ankara 06800, Turkey;* orcid.org/0000-0001-6898-7700; Email: onses@erciyes.edu.tr

Evren Mutlugun − *Department of Electrical and Electronics Engineering, Abdullah Gul University, Kayseri 38080, Turkey; UNAM—Institute of Materials Science and Nanotechnology, Bilkent University, Ankara 06800, Turkey;* orcid.org/0000-0003-3715-5594; Email: evren.mutlugun@agu.edu.tr

Authors

Sema Karabel Ocal − *ERNAM—Nanotechnology Research and Application Center, Erciyes University, Kayseri 38039, Turkey; Department of Materials Science and Engineering, Erciyes University, Kayseri 38039, Turkey*

N. Burak Kiremitler − *ERNAM—Nanotechnology Research and Application Center, Erciyes University, Kayseri 38039, Turkey; Department of Materials Science and Engineering, Erciyes University, Kayseri 38039, Turkey;* orcid.org/0000-0001-6065-4899

Ahmet Faruk Yazici − *Department of Nanotechnology Engineering, Abdullah Gul University, Kayseri 38080, Turkey*

Nusret Celik − *ERNAM—Nanotechnology Research and Application Center, Erciyes University, Kayseri 38039, Turkey; Department of Materials Science and Engineering, Erciyes University, Kayseri 38039, Turkey*

Complete contact information is available at: https://pubs.acs.org/10.1021/acsanm.2c00224

Notes

The authors declare no competing financial interest.

ACKNOWLEDGMENTS

This work was supported by the Research Fund of the Erciyes University (Project FDK-2020-10082). M.S.O. and E.M. acknowledge partial support from The Science Academy, Turkey, through the Young Scientist Award Program. S.K.O. acknowledges support through a Ph.D. scholarship (YOK 100/2000) from the Council of Higher Education, Turkey.

REFERENCES

(1) Protesescu, L.; Yakunin, S.; Bodnarchuk, M. I.; Krieg, F.; Caputo, R.; Hendon, C. H.; Yang, R. X.; Walsh, A.; Kovalenko, M. V. Nanocrystals of Cesium Lead Halide Perovskites (CsPbX3, X = Cl, Br, and I): Novel Optoelectronic Materials Showing Bright Emission with Wide Color Gamut. *Nano Lett.* **2015**, *15* (6), 3692−3696.

(2) Akkerman, Q. A.; Gandini, M.; Di Stasio, F.; Rastogi, P.; Palazon, F.; Bertoni, G.; Ball, J. M.; Prato, M.; Petrozza, A.; Manna, L. Strongly Emissive Perovskite Nanocrystal Inks for High-Voltage Solar Cells. *Nat. Energy* **2017**, *2* (2), 16194.

(3) Torun, I.; Altintas, Y.; Yazici, A. F.; Mutlugun, E.; Onses, M. S. Solid-State Encapsulation and Color Tuning in Films of Cesium Lead Halide Perovskite Nanocrystals for White Light Generation. *ACS Appl. Nano Mater.* **2019**, *2* (3), 1185−1193.

(4) Kim, Y. H.; Wolf, C.; Kim, Y. T.; Cho, H.; Kwon, W.; Do, S.; Sadhanala, A.; Park, C. G.; Rhee, S. W.; Im, S. H.; Friend, R. H.; Lee, T. W. Highly Efficient Light-Emitting Diodes of Colloidal Metal-Halide Perovskite Nanocrystals beyond Quantum Size. *ACS Nano* **2017**, *11* (7), 6586−6593.

(5) Chang, S.; Bai, Z.; Zhong, H. In Situ Fabricated Perovskite Nanocrystals: A Revolution in Optical Materials. *Advanced Optical Materials* **2018**, *6* (18), 1800380.

(6) Jancik Prochazkova, A.; Salinas, Y.; Yumusak, C.; Scharber, M. C.; Brüggemann, O.; Weiter, M.; Sariciftci, N. S.; Krajcovic, J.; Kovalenko, A. Controlling Quantum Confinement in Luminescent Perovskite Nanoparticles for Optoelectronic Devices by the Addition of Water. *ACS Appl. Nano Mater.* **2020**, *3* (2), 1242−1249.

(7) Song, J.; Li, J.; Li, X.; Xu, L.; Dong, Y.; Zeng, H. Quantum Dot Light-Emitting Diodes Based on Inorganic Perovskite Cesium Lead Halides (CsPbX3). *Adv. Mater.* **2015**, *27* (44), 7162−7167.

(8) Altintas, Y.; Torun, I.; Yazici, A. F.; Beskazak, E.; Erdem, T.; Serdar Onses, M.; Mutlugun, E. Multiplexed Patterning of Cesium Lead Halide Perovskite Nanocrystals by Additive Jet Printing for Efficient White Light Generation. *Chem. Eng. J.* **2020**, *380*, 122493.

(9) Begum, R.; Chin, X. Y.; Damodaran, B.; Hooper, T. J. N.; Mhaisalkar, S.; Mathews, N. Cesium Lead Halide Perovskite Nanocrystals Prepared by Anion Exchange for Light-Emitting Diodes. *ACS Appl. Nano Mater.* **2020**, *3* (2), 1766−1774.

(10) Wang, Y.; Li, X.; Song, J.; Xiao, L.; Zeng, H.; Sun, H. All-Inorganic Colloidal Perovskite Quantum Dots: A New Class of Lasing

Materials with Favorable Characteristics. *Adv. Mater.* **2015**, *27* (44), 7101−7108.
(11) Wang, X.; Shoaib, M.; Wang, X.; Zhang, X.; He, M.; Luo, Z.; Zheng, W.; Li, H.; Yang, T.; Zhu, X.; Ma, L.; Pan, A. High-Quality In-Plane Aligned CsPbX3 Perovskite Nanowire Lasers with Composition-Dependent Strong Exciton-Photon Coupling. *ACS Nano* **2018**, *12* (6), 6170−6178.
(12) Hu, L.; Zhao, Q.; Huang, S.; Zheng, J.; Guan, X.; Patterson, R.; Kim, J.; Shi, L.; Lin, C. H.; Lei, Q.; Chu, D.; Tao, W.; Cheong, S.; Tilley, R. D.; Ho-Baillie, A. W. Y.; Luther, J. M.; Yuan, J.; Wu, T. Flexible and Efficient Perovskite Quantum Dot Solar Cells via Hybrid Interfacial Architecture. *Nat. Commun.* **2021**, *12* (1), 1−9.
(13) Hazarika, A.; Zhao, Q.; Gaulding, E. A.; Christians, J. A.; Dou, B.; Marshall, A. R.; Moot, T.; Berry, J. J.; Johnson, J. C.; Luther, J. M. Perovskite Quantum Dot Photovoltaic Materials beyond the Reach of Thin Films: Full-Range Tuning of A-Site Cation Composition. *ACS Nano* **2018**, *12*, 10327.
(14) Khan, J.; Zhang, X.; Yuan, J.; Wang, Y.; Shi, G.; Patterson, R.; Shi, J.; Ling, X.; Hu, L.; Wu, T.; Dai, S.; Ma, W. Tuning the Surface-Passivating Ligand Anchoring Position Enables Phase Robustness in CsPbI3Perovskite Quantum Dot Solar Cells. *ACS Energy Lett.* **2020**, *5* (10), 3322−3329.
(15) Li, F.; Zhou, S.; Yuan, J.; Qin, C.; Yang, Y.; Shi, J.; Ling, X.; Li, Y.; Ma, W. Perovskite Quantum Dot Solar Cells with 15.6% Efficiency and Improved Stability Enabled by an α-CsPbI3/FAPbI3 Bilayer Structure. *ACS Energy Lett.* **2019**, *4* (11), 2571−2578.
(16) Ramasamy, P.; Lim, D. H.; Kim, B.; Lee, S. H.; Lee, M. S.; Lee, J. S. All-Inorganic Cesium Lead Halide Perovskite Nanocrystals for Photodetector Applications. *Chem. Commun.* **2016**, *52* (10), 2067−2070.
(17) Xia, M.; Zhu, S.; Luo, J.; Xu, Y.; Tian, P.; Niu, G.; Tang, J. Ultrastable Perovskite Nanocrystals in All-Inorganic Transparent Matrix for High-Speed Underwater Wireless Optical Communication. *Adv. Opt. Mater.* **2021**, *9*, 2002239.
(18) Li, X.; Wu, Y.; Zhang, S.; Cai, B.; Gu, Y.; Song, J.; Zeng, H. CsPbX3 Quantum Dots for Lighting and Displays: Roomerature Synthesis, Photoluminescence Superiorities, Underlying Origins and White Light-Emitting Diodes. *Adv. Funct. Mater.* **2016**, *26* (15), 2435−2445.
(19) Chan, K. K.; Giovanni, D.; He, H.; Sum, T. C.; Yong, K. T. Water-Stable All-Inorganic Perovskite Nanocrystals with Nonlinear Optical Properties for Targeted Multiphoton Bioimaging. *ACS Appl. Nano Mater.* **2021**, *4* (9), 9022−9033.
(20) Guo, X. X.; Tang, S. F.; Mu, Y. F.; Wu, L. Y.; Dong, G. X.; Zhang, M. Engineering a CsPbBr3-Based Nanocomposite for Efficient Photocatalytic CO2 Reduction: Improved Charge Separation Concomitant with Increased Activity Sites. *RSC Adv.* **2019**, *9* (59), 34342−34348.
(21) Mollick, S.; Mandal, T. N.; Jana, A.; Fajal, S.; Desai, A. V.; Ghosh, S. K. Ultrastable Luminescent Hybrid Bromide Perovskite@MOF Nanocomposites for the Degradation of Organic Pollutants in Water. *ACS Appl. Nano Mater.* **2019**, *2* (3), 1333−1340.
(22) Xu, L.; Chen, J.; Song, J.; Li, J.; Xue, J.; Dong, Y.; Cai, B.; Shan, Q.; Han, B.; Zeng, H. Double-Protected All-Inorganic Perovskite Nanocrystals by Crystalline Matrix and Silica for Triple-Modal Anti-Counterfeiting Codes. *ACS Appl. Mater. Interfaces* **2017**, *9* (31), 26556−26564.
(23) Pan, A.; Li, Y.; Wu, Y.; Yan, K.; Jurow, M. J.; Liu, Y.; He, L. Stable Luminous Nanocomposites of CsPbX 3 Perovskite Nanocrystals Anchored on Silica for Multicolor Anti-Counterfeit Ink and White-LEDs. *Mater. Chem. Front.* **2019**, *3* (3), 414−419.
(24) Feng, P.; Yang, X.; Feng, X.; Zhao, G.; Li, X.; Cao, J.; Tang, Y.; Yan, C. H. Highly Stable Perovskite Quantum Dots Modified by Europium Complex for Dual-Responsive Optical Encoding. *ACS Nano* **2021**, *15*, 6266.
(25) Yakunin, S.; Chaaban, J.; Benin, B. M.; Cherniukh, I.; Bernasconi, C.; Landuyt, A.; Shynkarenko, Y.; Bolat, S.; Hofer, C.; Romanyuk, Y. E.; Cattaneo, S.; Pokutnyi, S. I.; Schaller, R. D.; Bodnarchuk, M. I.; Poulikakos, D.; Kovalenko, M. V. Radiative Lifetime-Encoded Unicolour Security Tags Using Perovskite Nanocrystals. *Nat. Commun.* **2021**, *12* (1), 1−8.
(26) Zhang, F.; Shi, Z.; Li, S.; Ma, Z.; Li, Y.; Wang, L.; Wu, D.; Tian, Y.; Du, G.; Li, X.; Shan, C. Synergetic Effect of the Surfactant and Silica Coating on the Enhanced Emission and Stability of Perovskite Quantum Dots for Anticounterfeiting. *ACS Appl. Mater. Interfaces* **2019**, *11* (31), 28013−28022.
(27) Kovalenko, M. V.; Protesescu, L.; Bodnarchuk, M. I. Properties and Potential Optoelectronic Applications of Lead Halide Perovskite Nanocrystals. *Science* **2017**, *358*, 745−750.
(28) Huang, H.; Bodnarchuk, M. I.; Kershaw, S. V.; Kovalenko, M. V.; Rogach, A. L. Lead Halide Perovskite Nanocrystals in the Research Spotlight: Stability and Defect Tolerance. *ACS Energy Letters* **2017**, *2*, 2071−2083.
(29) Lou, S.; Xuan, T.; Wang, J. Stability: A Desiderated Problem for the Lead Halide Perovskites. *Opt. Mater. X* **2019**, *1*, 100023.
(30) Pan, J.; Shang, Y.; Yin, J.; De Bastiani, M.; Peng, W.; Dursun, I.; Sinatra, L.; El-Zohry, A. M.; Hedhili, M. N.; Emwas, A. H.; Mohammed, O. F.; Ning, Z.; Bakr, O. M. Bidentate Ligand-Passivated CsPbI 3 Perovskite Nanocrystals for Stable Near-Unity Photoluminescence Quantum Yield and Efficient Red Light-Emitting Diodes. *J. Am. Chem. Soc.* **2018**, *140* (2), 562−565.
(31) Xuan, T.; Yang, X.; Lou, S.; Huang, J.; Liu, Y.; Yu, J.; Li, H.; Wong, K. L.; Wang, C.; Wang, J. Highly Stable CsPbBr3 Quantum Dots Coated with Alkyl Phosphate for White Light-Emitting Diodes. *Nanoscale* **2017**, *9* (40), 15286−15290.
(32) Wei, Y.; Cheng, Z.; Lin, J. An Overview on Enhancing the Stability of Lead Halide Perovskite Quantum Dots and Their Applications in Phosphor-Converted LEDs. *Chemical Society Reviews* **2019**, *48*, 310−350.
(33) Ravi, V. K.; Scheidt, R. A.; Nag, A.; Kuno, M.; Kamat, P. V. To Exchange or Not to Exchange. Suppressing Anion Exchange in Cesium Lead Halide Perovskites with PbSO4-Oleate Capping. *ACS Energy Lett.* **2018**, *3* (4), 1049−1055.
(34) Li, G.; Rivarola, F. W. R.; Davis, N. J. L. K.; Bai, S.; Jellicoe, T. C.; De La Peña, F.; Hou, S.; Ducati, C.; Gao, F.; Friend, R. H.; Greenham, N. C.; Tan, Z. K. Highly Efficient Perovskite Nanocrystal Light-Emitting Diodes Enabled by a Universal Crosslinking Method. *Adv. Mater.* **2016**, *28* (18), 3528−3534.
(35) Jing, Q.; Zhang, M.; Huang, X.; Ren, X.; Wang, P.; Lu, Z. Surface Passivation of Mixed-Halide Perovskite CsPb(Br:XI1-x)3 Nanocrystals by Selective Etching for Improved Stability. *Nanoscale* **2017**, *9* (22), 7391−7396.
(36) Palazon, F.; Akkerman, Q. A.; Prato, M.; Manna, L. X-Ray Lithography on Perovskite Nanocrystals Films: From Patterning with Anion-Exchange Reactions to Enhanced Stability in Air and Water. *ACS Nano* **2016**, *10* (1), 1224−1230.
(37) Hu, Y.; Kareem, S.; Dong, H.; Xiong, W.; Tian, S.; Shamsi, J.; Li, L.; Zhao, X.; Xie, Y. CsPbBr3@SiO2Core-Shell Nanoparticle Films for Superhydrophobic Coatings. *ACS Appl. Nano Mater.* **2021**, *4* (6), 6306−6315.
(38) Palei, M.; Imran, M.; Biffi, G.; Manna, L.; Di Stasio, F.; Krahne, R. Robustness to High Temperatures of Al2O3-Coated CsPbBr3Nanocrystal Thin Films with High-Photoluminescence Quantum Yield for Light Emission. *ACS Appl. Nano Mater.* **2020**, *3* (8), 8167−8175.
(39) Li, Z. J.; Hofman, E.; Li, J.; Davis, A. H.; Tung, C. H.; Wu, L. Z.; Zheng, W. Photoelectrochemically Active and Environmentally Stable Cspbbr3/Tio2 Core/Shell Nanocrystals. *Adv. Funct. Mater.* **2018**, *28* (1), 1704288.
(40) Liu, H.; Tan, Y.; Cao, M.; Hu, H.; Wu, L.; Yu, X.; Wang, L.; Sun, B.; Zhang, Q. Fabricating CsPbX3-Based Type i and Type II Heterostructures by Tuning the Halide Composition of Janus CsPbX3/ZrO2 Nanocrystals. *ACS Nano* **2019**, *13* (5), 5366−5374.
(41) Song, P.; Qiao, B.; Song, D.; Cao, J.; Shen, Z.; Zhang, G.; Xu, Z.; Zhao, S.; Wageh, S.; Al-Ghamdi, A. Enhancing the Stability and Water Resistance of CsPbBr3 Perovskite Nanocrystals by Using Tetrafluoride and Zinc Oxide as Protective Capsules. *J. Mater. Sci.* **2020**, *55* (23), 9739−9747.

https://doi.org/10.1021/acsanm.2c00224
ACS Appl. Nano Mater. 2022, 5, 6201−6212

(42) Cheng, H.; Yin, Y.; Tang, J.; Fan, D.; Huang, J. J.; Jin, S. Water-Assisted Synthesis of Highly Stable CsPbX3perovskite Quantum Dots Embedded in Zeolite-Y. *RSC Adv.* **2021**, *11* (5), 2866−2871.
(43) Zhao, S.; Fu, S.; He, P.; Cui, J.; Yu, X.; Liang, J.; Duan, X.; Chen, D.; Bonn, M.; Wang, H. I.; Jia, D.; Yang, Z.; Zhou, Y. Geopolymer-Encapsulated Cesium Lead Bromide Perovskite Nanocrystals for Potential Display Applications. *ACS Appl. Nano Mater.* **2020**, *3* (12), 11695−11700.
(44) Liao, H.; Guo, S.; Cao, S.; Wang, L.; Gao, F.; Yang, Z.; Zheng, J.; Yang, W. A General Strategy for In Situ Growth of All-Inorganic CsPbX3 (X = Br, I, and Cl) Perovskite Nanocrystals in Polymer Fibers toward Significantly Enhanced Water/Thermal Stabilities. *Adv. Opt. Mater.* **2018**, *6* (15), 1800346.
(45) Zhou, Q.; Bai, Z.; Lu, W. G.; Wang, Y.; Zou, B.; Zhong, H. In Situ Fabrication of Halide Perovskite Nanocrystal-Embedded Polymer Composite Films with Enhanced Photoluminescence for Display Backlights. *Adv. Mater.* **2016**, *28* (41), 9163−9168.
(46) Xin, Y.; Zhao, H.; Zhang, J. Highly Stable and Luminescent Perovskite-Polymer Composites from a Convenient and Universal Strategy. *ACS Appl. Mater. Interfaces* **2018**, *10* (5), 4971−4980.
(47) Boussoufi, F.; Pousthomis, M.; Kuntzmann, A.; D'Amico, M.; Patriarche, G.; Dubertret, B. Spray-Drying Polymer Encapsulation of CsPbBr3Perovskite Nanocrystals with Enhanced Photostability for LED Downconverters. *ACS Appl. Nano Mater.* **2021**, *4* (7), 7502−7512.
(48) Liu, H.; Siron, M.; Gao, M.; Lu, D.; Bekenstein, Y.; Zhang, D.; Dou, L.; Alivisatos, A. P.; Yang, P. Lead Halide Perovskite Nanowires Stabilized by Block Copolymers for Langmuir-Blodgett Assembly. *Nano Res.* **2020**, *13* (5), 1453−1458.
(49) Gomez, L.; De Weerd, C.; Hueso, J. L.; Gregorkiewicz, T. Color-Stable Water-Dispersed Cesium Lead Halide Perovskite Nanocrystals. *Nanoscale* **2017**, *9* (2), 631−636.
(50) Wu, H.; Lin, S.; Wang, R.; You, X.; Chi, Y. Water-Stable and Ion Exchange-Free Inorganic Perovskite Quantum Dots Encapsulated in Solid Paraffin and Their Application in Light Emitting Diodes. *Nanoscale* **2019**, *11* (12), 5557−5563.
(51) de Mello, J. C.; Wittmann, H. F.; Friend, R. H. An Improved Experimental Determination of External Photoluminescence Quantum Efficiency. *Adv. Mater.* **1997**, *9* (3), 230−232.
(52) Rojas, J.; Cabrera, S.; Benavides, J.; Lopera, Y.; Yarce, C. J. Lipidic Matrixes Containing Clove Essential Oil: Biological Activity, Microstructural and Textural Studies. *Molecules* **2021**, *26* (9), 2425.
(53) Freitas, C. A. S.; Vieira, Í. G. P.; Sousa, P. H. M.; Muniz, C. R.; Gonzaga, M. L. D. C.; Guedes, M. I. F. Carnauba Wax P-Methoxycinnamic Diesters: Characterisation, Antioxidant Activity and Simulated Gastrointestinal Digestion Followed by in Vitro Bioaccessibility. *Food Chem.* **2016**, *196*, 1293−1300.
(54) Robertson, D.; van Reenen, A.; Duveskog, H. A Comprehensive Investigation into the Structure-Property Relationship of Wax and How It Influences the Properties of Hot Melt Adhesives. *Int. J. Adhes. Adhes.* **2020**, *99*, 102559.
(55) Farber, C.; Li, J.; Hager, E.; Chemelewski, R.; Mullet, J.; Rogachev, A. Y.; Kurouski, D. Complementarity of Raman and Infrared Spectroscopy for Structural Characterization of Plant Epicuticular Waxes. *ACS Omega* **2019**, *4* (2), 3700−3707.
(56) Banski, M.; Afzaal, M.; Malik, M. A.; Podhorodecki, A.; Misiewicz, J.; O'Brien, P. Special Role for Zinc Stearate and Octadecene in the Synthesis of Luminescent ZnSe Nanocrystals. *Chem. Mater.* **2015**, *27* (11), 3797−3800.
(57) Jiang, G.; Guhrenz, C.; Kirch, A.; Sonntag, L.; Bauer, C.; Fan, X.; Wang, J.; Reineke, S.; Gaponik, N.; Eychmüller, A. Highly Luminescent and Water-Resistant CsPbBr3-CsPb2Br5 Perovskite Nanocrystals Coordinated with Partially Hydrolyzed Poly(Methyl Methacrylate) and Polyethylenimine. *ACS Nano* **2019**, *13* (9), 10386−10396.
(58) Li, T. Y.; Xu, X.; Lin, C. H.; Guan, X.; Hsu, W. H.; Tsai, M. L.; Fang, X.; Wu, T.; He, J. H. Highly UV Resistant Inch-Scale Hybrid Perovskite Quantum Dot Papers. *Adv. Sci.* **2020**, *7* (17), 1902439.
(59) Ren, J.; Dong, X.; Zhang, G.; Li, T.; Wang, Y. Air-Stable and Water-Resistant All-Inorganic Perovskite Quantum Dot Films for White-Light-Emitting Applications. *New J. Chem.* **2017**, *41* (22), 13961−13967.
(60) Cao, P.; Yang, B.; Zheng, F.; Wang, L.; Zou, J. High Stability of Silica-Wrapped CsPbBr3 Perovskite Quantum Dots for Light Emitting Application. *Ceram. Int.* **2020**, *46* (3), 3882−3888.
(61) Yang, D.; Li, X.; Zeng, H. Surface Chemistry of All Inorganic Halide Perovskite Nanocrystals: Passivation Mechanism and Stability. *Advanced Materials Interfaces* **2018**, *5* (8), 1701662.
(62) Pan, A.; He, B.; Fan, X.; Liu, Z.; Urban, J. J.; Alivisatos, A. P.; He, L.; Liu, Y. Insight into the Ligand-Mediated Synthesis of Colloidal CsPbBr3 Perovskite Nanocrystals: The Role of Organic Acid, Base, and Cesium Precursors. *ACS Nano* **2016**, *10* (8), 7943−7954.
(63) Celik, N.; Kiremitler, N. B.; Ruzi, M.; Onses, M. S. Waxing the Soot: Practical Fabrication of All-Organic Superhydrophobic Coatings from Candle Soot and Carnauba Wax. *Prog. Org. Coatings* **2021**, *153*, 106169.
(64) Rao, L.; Tang, Y.; Song, C.; Xu, K.; Vickers, E. T.; Bonabi Naghadeh, S.; Ding, X.; Li, Z.; Zhang, J. Z. Polar-Solvent-Free Synthesis of Highly Photoluminescent and Stable CsPbBr 3 Nanocrystals with Controlled Shape and Size by Ultrasonication. *Chem. Mater.* **2019**, *31*, 365.
(65) Pekarovicova, A.; Bhide, H.; Fleming, P. D.; Pekarovic, J. Phase-Change Inks. *J. Coatings Technol. 2003 75936* **2003**, *75* (936), 65−72.
(66) Chiang, C. K.; Kurniawan, A.; Kao, C. Y.; Wang, M. J. Single Step and Mask-Free 3D Wax Printing of Microfluidic Paper-Based Analytical Devices for Glucose and Nitrite Assays. *Talanta* **2019**, *194*, 837−845.
(67) Raoufi, M. A.; Razavi Bazaz, S.; Niazmand, H.; Rouhi, O.; Asadnia, M.; Razmjou, A.; Ebrahimi Warkiani, M. Fabrication of Unconventional Inertial Microfluidic Channels Using Wax 3D Printing. *Soft Matter* **2020**, *16* (10), 2448−2459.
(68) Soda, M.; Beyene, A. Multiphase Ultra-Low Grade Thermal Energy Storage for Organic Rankine Cycle. *Int. J. Energy Res.* **2016**, *40* (1), 51−60.
(69) Zhao, Y.; Thapa, S.; Weiss, L.; Lvov, Y. Phase Change Heat Insulation Based on Wax-Clay Nanotube Composites. *Adv. Eng. Mater.* **2014**, *16* (11), 1391−1399.

https://doi.org/10.1021/acsanm.2c00224
ACS Appl. Nano Mater. 2022, 5, 6201−6212